

Discovery of Two Highly Scattered Pulsars from Image-Based Circular Polarization Searches with the Australian SKA Pathfinder

RAHUL SENGAR ^{1,2,3} DAVID L. KAPLAN ³ EMIL LENC ⁴ AKASH ANUMARLAPUDI ⁵ NATASHA HURLEY-WALKER ⁶
 ZITENG WANG ⁶ LAURA DRIESSEN ^{7,8} DOUGAL DOBIE ^{7,8} AND TARA MURPHY ^{7,8}

¹ *Max Planck Institute for Gravitational Physics (Albert Einstein Institute), D-30167 Hannover, Germany*

² *Leibniz Universität Hannover, D-30167 Hannover, Germany*

³ *Center for Gravitation, Cosmology, and Astrophysics, Department of Physics, University of Wisconsin-Milwaukee, P.O. Box 413, Milwaukee, WI 53201, USA*

⁴ *CSIRO Space and Astronomy, PO Box 76, Epping, NSW 1710, Australia*

⁵ *Department of Physics and Astronomy, University of North Carolina at Chapel Hill, 120 E. Cameron Ave, Chapel Hill, NC, 27599, USA*

⁶ *International Centre for Radio Astronomy Research, Curtin University, Kent St, Bentley WA 6102, Australia*

⁷ *Sydney Institute for Astronomy, School of Physics, The University of Sydney, New South Wales 2006, Australia*

⁸ *ARC Centre of Excellence for Gravitational Wave Discovery (OzGrav), Hawthorn, VIC 3122, Australia*

ABSTRACT

We report the discovery and timing of two pulsars from a sample of four circularly polarized sources identified in radio continuum images taken as part of the Australian SKA Pathfinder (ASKAP) Variables and Slow Transients (VAST) survey. Observations with the Parkes (Murriyang) radio telescope confirmed both sources as normal pulsars with high dispersion measures. PSR J1646–4451 has a spin period of 217 ms and a dispersion measure (DM) of 928 cm^{−3} pc, while PSR J1837–0616 exhibits a spin period of 118 ms and a DM of 793 cm^{−3} pc. These pulsars show extreme pulse broadening due to scattering, with measured scattering timescales of 290 ms and 343 ms at observing frequencies of 1.8 GHz and 1.9 GHz, respectively. These measurements imply extrapolated scattering timescales at 1 GHz of 2479 ms and 2154 ms, placing them among the most heavily scattered pulsars known to date. Our findings underscore the potential of using circular polarization in radio continuum images as a tool for identifying highly scattered pulsars. Future wide-field radio continuum surveys are poised to uncover a broader population of extreme pulsars particularly those that are heavily scattered at 1.4 GHz, intrinsically faint, or residing in binaries—offering valuable insights into both pulsar demographics and the complex structure of the interstellar medium.

Keywords: Neutron stars (1108); Galactic radio sources (571); Radio pulsars (1353); Interstellar scattering (854)

1. INTRODUCTION

The majority of pulsars have been discovered through time-domain-based, untargeted, and large-scale pulsar surveys that systematically scan wide regions of the sky in an unbiased manner (e.g., Manchester et al. 2001; Cordes et al. 2006; Keith et al. 2010; Keane et al. 2018; Han et al. 2021; Padmanabha et al. 2023; Stovall et al. 2014; Sanidas et al. 2019). The dedispersed time-series data are then searched for periodic signals using Fast Fourier Transform (e.g., Lorimer & Kramer 2004) or Fast Folding Algorithm (FFA; Staelin 1969) techniques. However, these searching algorithms result in hundreds of millions of candidates, majority of which arise from

radio frequency interference (RFI), noise, or statistical fluctuations that can mimic genuine pulsar signals. This necessitates substantial post-processing and candidate vetting efforts. If, however, one could *a priori* identify sources in the sky that are likely to be promising pulsar candidates, and subsequently conduct time-domain searches specifically for those sources, it could potentially yield significant gains in both computational efficiency and detection sensitivity. Such a targeted refinement of the standard blind-search approach could result in interesting pulsars while simultaneously reducing the volume of spurious candidates.

Radio continuum imaging surveys provide a complementary approach to pulsar searches by targeting their persistent, steep-spectrum emission (Jankowski et al. 2018), rather than relying solely on time-domain periodicity. This approach is particularly advantageous in scenarios where traditional time-domain searches are limited by propagation effects in the interstellar medium (ISM). When pulsar signals pass through an inhomogeneous interstellar medium, they suffer from temporal smearing due to multipath scattering (Sutton 1971). Unless the pulsar is sufficiently bright, its signal may be lost in background noise due to scattering. Observing pulsars at higher frequencies can mitigate this effect as scattering timescale decreases with increasing frequency i.e. $\tau \propto \nu^{-4}$ (Rickett 1977). However, due to the steep spectrum nature of the majority of pulsars and lower frequencies providing a larger field of view and thus faster survey speed, most large-scale time-domain surveys have been conducted at or below 1.4 GHz (e.g., Sengar et al. 2025, and references therein). But, it makes them particularly susceptible to scattering along the Galactic plane. Similarly, orbital modulation in binary pulsars smear out the pulsed signal and can significantly hinder detection if the effects of orbital acceleration are not properly accounted for (Johnston & Kulkarni 1991). Finally, ephemeral pulsars such as rotating radio transients (RRATs) (McLaughlin et al. 2006; Keane & McLaughlin 2011), eclipsing pulsars (Thompson et al. 1994), and nulling pulsars (Rickett 1990; Wang et al. 2007) also often evade detection due to their sporadic emission. Unlike time-series analyses, continuum observations integrate emission over long durations, effectively mitigating these effects.

Radio Continuum observations are particularly effective because, pulsars are highly polarized sources and exhibit distinctive polarization properties — typically a high degree of linear polarization (10–50%) and noticeable circular polarization (5–30%) (e.g., Wang et al. 2023; Oswald et al. 2023). These characteristics are rare among other extragalactic radio sources such as AGN and radio galaxies which are dominated by incoherent synchrotron emission with minimal circular polarization (e.g., Saikia & Salter 1988; Bjornsson 1990). Radio stars however show high fractional circular polarization (e.g., Pritchard et al. 2021), but the emission from them is narrow band (could be full band as well), transient and often linked to stellar counterparts detectable in optical/infrared surveys. Therefore, they can be easily distinguished from broadband emission of pulsars. The combination of these unique polarization

signatures with compact morphology and steep spectral indices ($\alpha \sim -1.6$, where $S_\nu \propto \nu^\alpha$ Jankowski et al. 2018) enables efficient identification of pulsar candidates in wide-field radio continuum images. This can significantly reduce the number of potential targets for follow-up. However, this target identification method does not guarantee pulsar detection as other source types may share some characteristics, especially when looking at outliers from large background populations. These candidate sources must ultimately be observed with high resolution radio data and analyzed using standard pulsar search techniques (e.g., FFT or FFA) to confirm their pulsar nature. Thus, radio continuum observations serve as a powerful filtering mechanism, converting traditional unbiased searches into more targeted campaigns. This approach is particularly valuable for discovering pulsars in challenging regimes—such as those in highly scattered regions or binary systems—that might otherwise be missed by conventional time-domain surveys. By pre-selecting the most promising circularly polarized candidates, radio continuum imaging significantly can improve the efficiency of pulsar searches.

In the last few decades, the use of radio continuum imaging for pulsar discovery has evolved significantly. Recent advances in radio astronomy instrumentation and interferometers have enabled a new generation of high-sensitivity, wide-bandwidth continuum surveys with unprecedented sky coverage and angular resolution. Facilities like the Australian SKA Pathfinder (ASKAP) with its Evolutionary Map of the Universe (EMU) survey (Norris et al. 2011), Murchison Widefield Array (Lenc et al. 2018), the Karl G. Jansky Very Large Array (VLA) conducting the VLA Sky Survey (VLASS; Lacy et al. 2020), Low-Frequency Array (LOFAR) Two-metre Sky Survey (LoTSS; Best et al. 2023), LOFAR’s TULIPP project (Sobey et al. 2022), and MeerKAT’s various survey programs (e.g., Fender et al. 2016; Padmanabhan et al. 2023) are producing deep, wide-field radio images ideal for identifying pulsar candidates through their spectral and polarization properties.

Several recent serendipitous discoveries of pulsars illustrate the growing effectiveness of this approach. For example, the identification of the highly polarized ASKAP source as millisecond pulsar PSR J1431–6328 previously missed in the High Time Resolution Universe survey due to scattering at L-band frequencies or processing errors (Kaplan et al. 2019). Similarly, MeerKAT observations during the 2020 Saturn-Jupiter conjunction serendipitously discovered the strongly scintillating PSR J2009–2026 (Zhu et al. 2024). Other examples include the discovery of a pulsar J0523–7125 in the Large Magellanic Clouds (Wang et al. 2022), discovery of a

Table 1. Observed properties of selected sources in VAST. The table lists the coordinates of each source, mean of total intensity (I_{mean}), circular polarization (V_{mean}), fractional circular polarization ($|V|/I$), and signal-to-noise ratio (S/N).

Source Name	RA (J2000)	DEC (J2000)	GL ($^{\circ}$)	GB ($^{\circ}$)	I_{mean} (mJy)	V_{mean} (mJy)	$ V /I$	S/N	K_s	Type
									(AB)	
ASKAP J162048.8–492745	16:20:48.88(1)	–49:27:45(3)	333.900	0.391	2.5	0.51	0.27	4.1	16.99 ± 0.01	star
ASKAP J164634.5–445126	16:46:34.52(1)	–44:51:26(3)	340.250	0.305	2.4	–0.45	0.19	5.7	>22.2	pulsar
ASKAP J183233.4–080835	18:32:33.40(1)	–08:08:35(3)	23.538	0.453	2.3	0.47	0.26	3.3	>22.3	unknown
ASKAP J183720.9–061609	18:37:20.90(1)	–06:16:09(3)	25.747	0.264	13.2	0.96	0.07	10.0	>20.8	pulsar

young pulsar PSR J1032–5804 through its circular polarization, despite its high dispersion measure (800 pc cm $^{-3}$) and rotation measure (Wang et al. 2024), candidate redback pulsar binary 4FGL J1646.5–4406 (Zic et al. 2024), and a highly scattered PSR J1631–4722 associated with supernova remnant G336.7+0.5 and identified as an compact source (RACS J163159.8–472157) with tail-like emission in the Rapid ASKAP Continuum Survey (McConnell et al. 2020), with pulsations discovered by Ahmad et al. (2025). Most recently, a new RRAT (Mcsweeney et al. 2025) and four eclipsing MSPs (Petrou et. al., accepted) have been discovered using image based searches.

These discoveries highlight three critical advantages of continuum imaging: (1) immunity to scattering effects that can limit time-domain searches, (2) sensitivity to polarization properties that serve as unique pulsar fingerprints, and (3) ability to identify pulsars in complex environments like supernova remnants. Statistical analyses now suggest that image-based methods may uncover pulsar populations complementary to those found via periodicity searches (Frail et al. 2024). The growing sample of these highly scattered and young pulsars demonstrates that image based searches will be essential for a complete census of the Galactic pulsar population. Future surveys with the SKA and its precursors are expected to increase the yield of image-discovered pulsars by an order of magnitude, especially in the challenging Galactic plane region where traditional searches are least effective (Dai et al. 2018).

In this paper, we present the discovery of two highly scattered pulsars — PSR J1646–4451 and PSR J1837–0616 — which are among a sample of four circularly polarized sources detected in the ASKAP Variable and Slow Transients (VAST) survey (Murphy et al. 2013, 2021) and were subsequently confirmed as pulsars with the Parkes radio telescope. In Section 2, we summarize the discovery observations both in the radio continuum data using circular polarization based search as well as in radio Parkes data using the periodicity searches.

Timing analysis, polarimetry, and scattering analysis are discussed in Section 3. Finally, the discussion and conclusion are presented in Sections 4 and 5.

2. PULSAR CANDIDATE IDENTIFICATION

2.1. VAST observations

Since November 2022, the VAST project has been conducting a radio survey using ASKAP which targets the southern the Galactic plane. This campaign systematically monitored 41 preselected sky regions, each constrained to Galactic latitudes within $\pm 6^{\circ}$ and declinations below -10° (although the exact selection has changed slightly over time), cumulatively spanning around 1260 square degrees. Observations of these regions were repeated approximately every fortnight. Each session involved a 12-minute exposure at a central frequency of 888 MHz and employed a bandwidth of 288 MHz, enabling a median sensitivity of roughly 0.2 mJy beam $^{-1}$ in areas along the plane.

The polarization data used are standard ASKAP data products, in which all instrumental correlations (XX, XY, YX, and YY) are recorded for reconstruction of images in all four Stokes parameters: I , Q , U , and V . Data handling was performed offline through the untargeted VAST pipeline, yielding both total intensity and circular polarization images, along with corresponding source catalogs. The bandpass and flux calibration relied on PKS B1934–638, and temporal phase variations were corrected via self-calibration procedures. The details of these processing steps are outlined in Murphy et al. (2021).

We focused our analysis on detecting compact sources with high fractional circular polarization, aiming to isolate targets of astrophysical interest, potentially pulsars. After rejecting sources with known multi-wavelength matches most of which are radio stars (Pritchard et al. 2021; Driessen et al. 2024a) or known pulsars, we identified four circularly polarized sources for followup (see Table 1) whose degree of fractional circular polarization

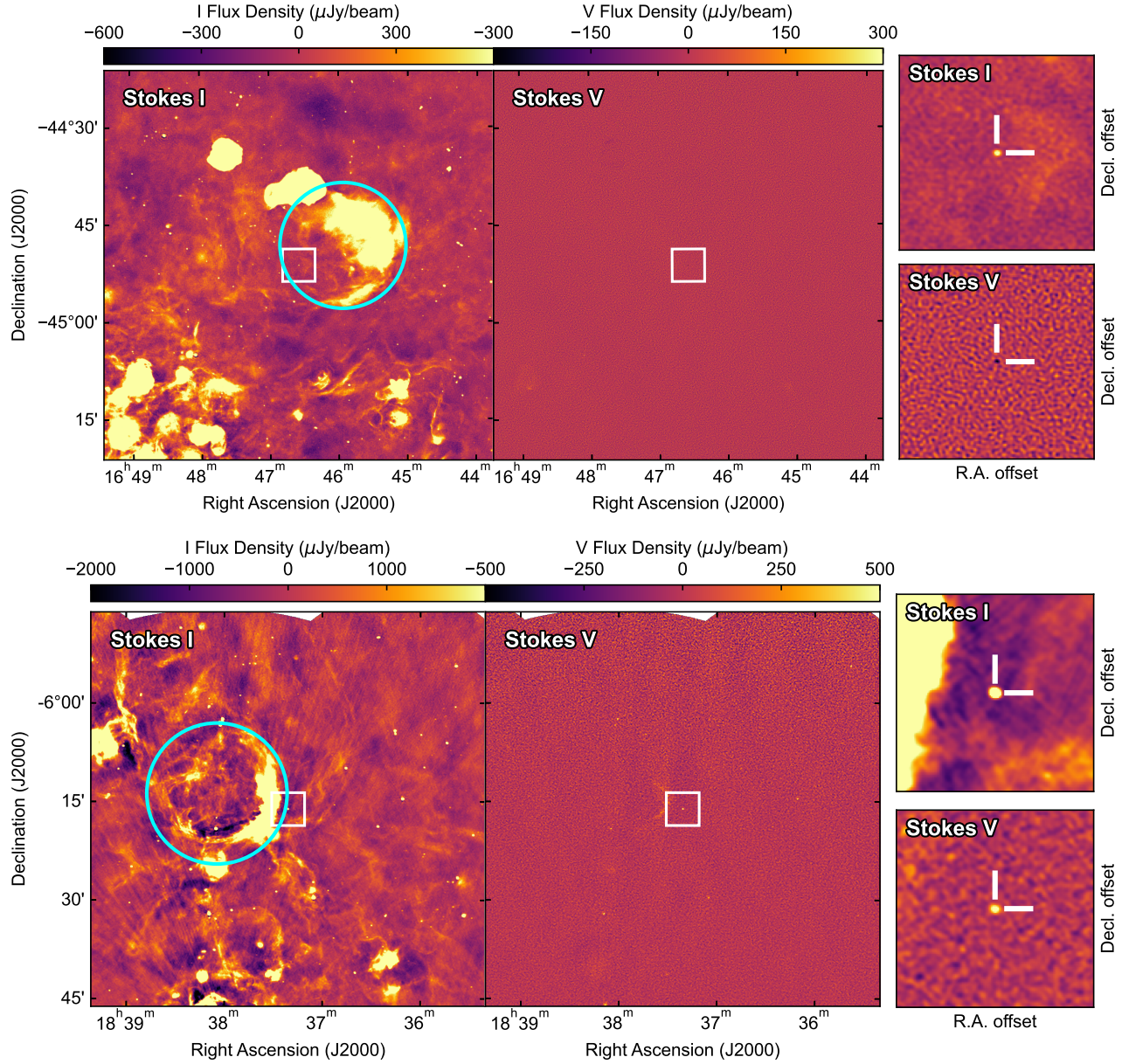


Figure 1. ASKAP radio continuum images of the fields centered on two pulsars at 888 MHz: PSR J1646–4451 (top panels) and PSR J1837–0616 (bottom panels). For each field, the Stokes I image (left) shows the total intensity emission, revealing extended Galactic structure and diffuse background emission, while the Stokes V image (middle) displays the circularly polarized intensity. The white squares mark the known positions of the pulsars. The panels on the right show zoomed-in views centered on the pulsar positions in both Stokes I and V, with the pulsar location indicated by white crosshairs. These images have been corrected for the ASKAP primary beam response, and the color bars denote the flux density scales in $\mu\text{Jy beam}^{-1}$. Cyan ellipses indicate the HII regions WISE G340.216+00.424 (top) and WISE G025.867+00.118 (bottom).

is between 7% and 30%, similar to what is seen in pulsars (Anumarlapudi et al. 2023).

2.2. Multi-wavelength search for counterparts

Sources at radio wavelengths that show significant polarization ($\gtrsim 5\text{--}10\%$) often include stars (Pritchard et al. 2021), pulsars (Anumarlapudi et al. 2023), and white dwarf binaries, especially magnetic cataclysmic variables

(MCVs; Barrett et al. 2020). Hence, we searched the archival optical and near infrared (NIR) data for these sources that might inform us of their nature. At optical wavelengths, we searched the data from *Gaia* (Gaia Collaboration et al. 2023), the Dark Energy Camera Plane Survey (DECaPS; Saydjari et al. 2023, where available), and the Panoramic Survey Telescope and Rapid Response System (Pan-STARRS; Chambers et al. 2016,

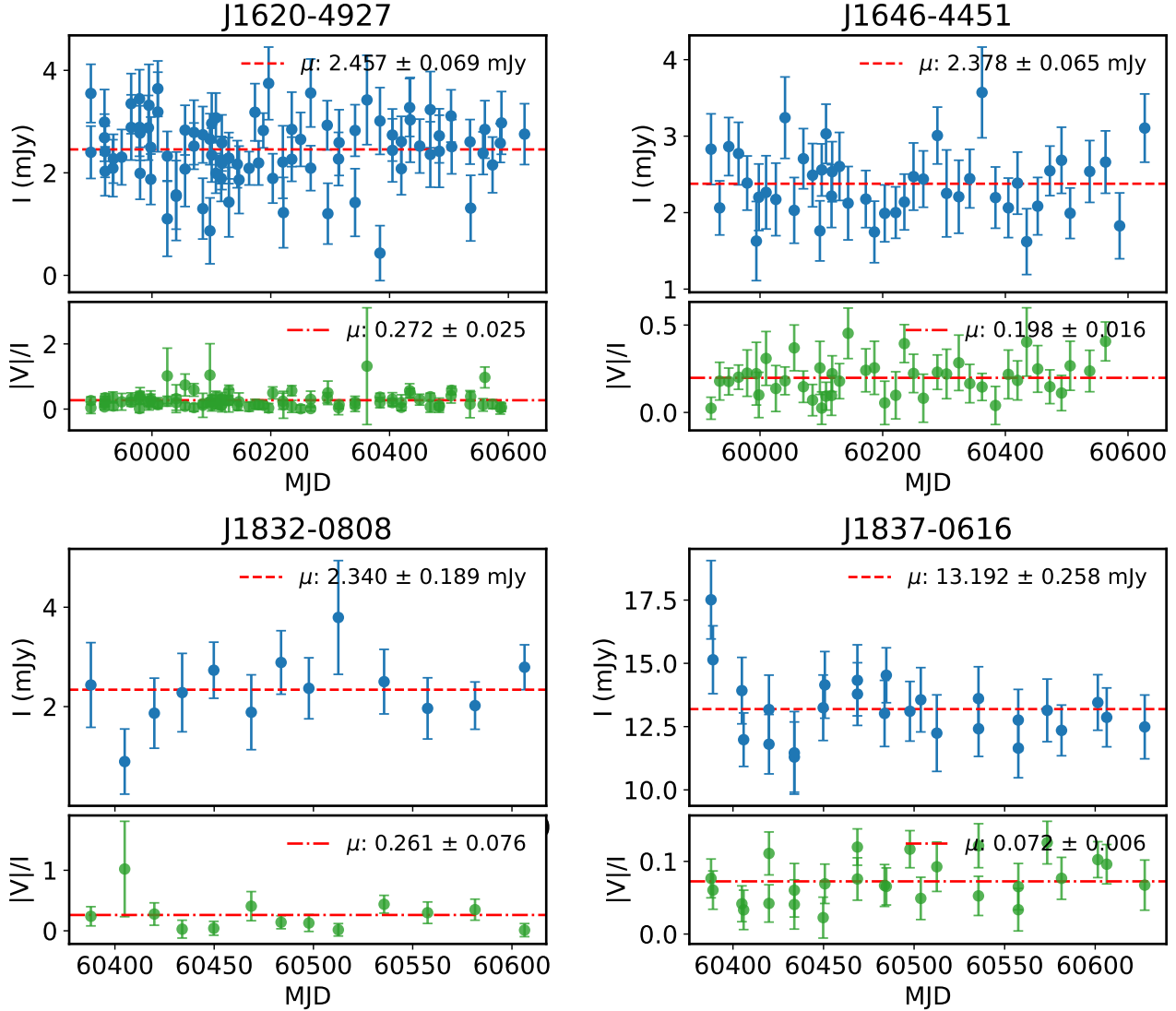


Figure 2. Total intensity (I , top panels) and circular polarization (V , bottom panels) as a function of MJD for four circularly polarized sources. Each point represents a single observation, with error bars denoting measurement uncertainties. The red dashed lines corresponds to the mean flux densities in I and V . The sources exhibit stable fluxes and polarization over time, without too much variation.

where DECaPS data were not available). At NIR wavelengths, we searched deep observations from the VISTA Variables in the Vía Láctea Survey (VVV; [Catelan et al. 2011](#)) and the Galactic Plane Survey from the UKIRT Infrared Deep Sky Survey (UKIDSS; [Lawrence et al. 2007](#)). At NIR wavelengths, often multiple short scans are available, and hence, we stacked these observations (or used the stacked image, if available) to obtain deeper observations. At the location of these sources, we performed aperture photometry on the stacked images to get source fluxes/upper limits. Zero-point calibration for the stacked images was performed using the DECaPS and UKIDSS source catalogs.

For J1620-4927, we identified the star *Gaia* DR3 5935425106911225216, $0.6''$ away from the radio position, well within the ASKAP position uncertainty. This star has G -band magnitude of 18.6, an effective temperature of 4200 K, and log surface gravity of 4.9. Considering the source density of sources in *Gaia* DR3 (in a $5'$ radius), we estimate the probability of random association with J1620-4927 to be 0.02. J1620-4927 is also well detected in the DECaPS and VVV data, with the broad band spectral energy distribution (from these colors) consistent with the temperature estimated by the *Gaia* survey. These parameters are similar to many of the K-type stars in the Sydney Radio Star Catalogue

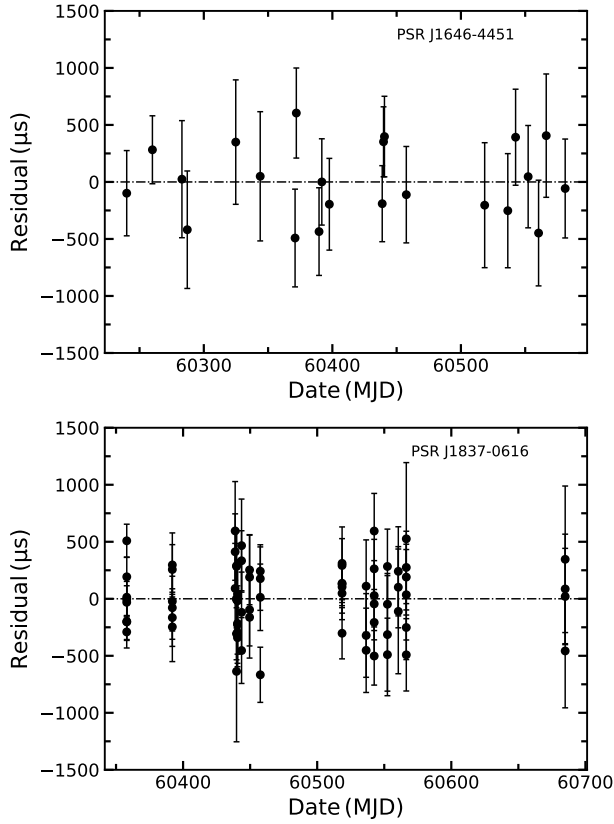


Figure 3. Timing residuals for PSR J1646–4451 and PSR J1837–0616 using Parkes data.

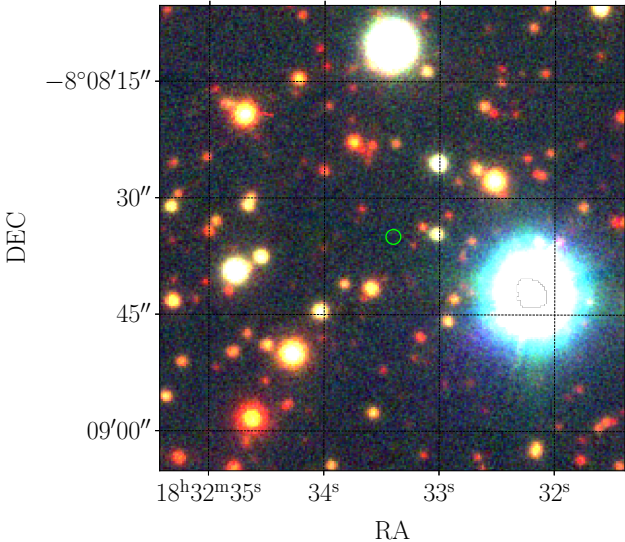


Figure 4. Optical *gri* composite image of the field of J1832–0808, using the data from DECaPS. The image is $30''$ in extent along both axes, and the lime circle shows the radio position of J1832–0808.

(Driessen et al. 2024b); however, no detectable parallax was measured for J1620–4927.

For J1646–4451, no optical counterpart was found, but we found a NIR source in the VVV images $0''.83$ away from the radio position. However, considering the higher source density at NIR wavelengths in the Galactic plane, we derive a probability of random association to be 0.4; hence, this association is likely not robust. Excluding this source, at the position of J1646–4451, in a $0.5''$ circle, we estimate an upper limit of $K_s=22.2$ AB.

For J1832–0808, and J1837–0616, no DECaPS/VVV data were available, and hence we inspected Pan-STARRS and UKIDSS data. In the case of J1832–0808, no counterpart was found either at optical or NIR wavelengths up to a K_s -band limiting magnitude of 22.3 AB. However, for J1837–0616, we found a NIR (but not optical) detection of a source, $1.3''$ away from the radio position. However, similar to J1646–4451, given the higher source density in the Galactic plane, we estimate the probability of random association to be 0.6 between the NIR source and J1837–0616. At the location of J1837–0616, we estimate the limiting magnitude to be $K_s > 20.8$ AB.

2.3. Murriyang observations and periodicity search

In order to confirm if any of these circularly polarized sources are pulsars, we conducted follow-up observations at the Parkes radio telescope using the Ultra-Wideband Low (UWL; Hobbs et al. 2020) receiver, which provides continuous frequency coverage from 704 MHz to 4032 MHz. The extensive bandwidth of the UWL system offers enhanced sensitivity to pulsars that may be undetectable at conventional L-band frequencies (e.g., 1000–1500 MHz), either due to low signal significance or strong interstellar scattering. Each source was observed in search mode (total intensity) for durations between 60 and 72 minutes, using a time resolution of 64 μ s, 2-bit sampling, and 500 kHz channel bandwidth, yielding a total of 6656 frequency channels. Periodicity searches were performed using the GPU-accelerated PEASOUP¹ software, which applies time-domain resampling techniques to improve sensitivity to binary pulsars experiencing orbital acceleration. A dispersion measure (DM) range of up to $1500 \text{ cm}^{-3} \text{ pc}$ was searched for each target, corresponding to 1.2–2.0 times the maximum DM predicted by either the NE2001 or YMW16 electron density models. The acceleration search covered a range of $\pm 25 \text{ ms}^{-2}$, sufficient to detect signals from highly accelerated binary systems.

¹ <https://github.com/ewanbarr/peasoup>

To exploit the wide frequency coverage of the UWL band receiver, we implemented a subbanded search strategy. Each observation was divided into 12 frequency subbands—eight segments of 400 MHz and four segments of 800 MHz—resulting in 60 independent datasets. Prior to searching, frequency masks for radio frequency interference (RFI) were generated using the `rfifind` suite from PRESTO² periodicity search code. Candidate selection following the acceleration search was performed according to the criteria established in (Sengar et al. 2023, 2025). Candidates were subsequently folded and diagnostic plots were generated using the `dspsr` and `pdmp` modules from the PSRCHIVE³ software package. Folded profiles with a signal-to-noise ratio (S/N) exceeding 8 for slow pulsars ($P > 100$ ms) and 10 for fast pulsars ($P < 100$ ms) were shortlisted for visual inspection. Out of the four observations, three yielded clear detections of pulsars. To verify whether these were previously known sources, we used the Pulsar Survey Scraper⁴ to cross-check positional matches. Two of the pulsars, PSRs J1646–4451 and J1837–0616, did not correspond to any published or catalogued sources and are therefore new pulsar detections (their corresponding radio continuum images are shown in Figure 1)

Both new pulsars are extremely faint and exhibit significant scattering below 1500 MHz. PSR J1646–4451 is particularly faint, and we initially detected it only in the 2400–3200 MHz and 3200–4000 MHz subbands with a signal-to-noise ratio (S/N) of approximately 13 in each subband. However, when the full 1500–4032 MHz band was coherently folded, the resulting folded S/N increased to 18. The full width at half maximum (FWHM) of the integrated pulse profile is approximately 10% of the pulse period. In contrast, PSR J1837–0616 was detected across all subbands above 1500 MHz. The folded S/N over the full 1500–4032 MHz band was 115, and the FWHM of its pulse profile is approximately 11%.

3. DATA ANALYSIS

3.1. *Timing Analysis*

Following the discovery of the two pulsars, we conducted a follow-up campaign under the Parkes project P1332, using the UWL receiver in conjunction with the MEDUSA backend. Observations were conducted

in search mode with full Stokes parameters along with noise diode observation before observing the pulsars. Data were recorded with a frequency resolution of 1 MHz per channel, yielding 3328 frequency channels, and a time resolution of $128\ \mu\text{s}$.

PSR J1646–4451 was discovered with a modest signal-to-noise ratio ($\text{S/N} \approx 20$) during a 72-minute observation. Consequently, subsequent follow-up observations of this source were integrated over durations ranging from 60 to 90 minutes to maintain the similar sensitivity in each observation. However, PSR J1837–0616, being intrinsically brighter, required only 5–10 minutes of integration to achieve high-quality detections.

Each observation was initially folded at the known spin period and dispersion measure (DM) using DSPSR, and the folding parameters were subsequently refined using PDMP. The resulting folded archives were cleaned using the CLFD⁵ software to mitigate RFI. Additionally, narrowband and impulsive RFI were excised manually using PAZI, part of the PSRCHIVE suite. Note that both pulsars exhibit strong scattering below 1500 MHz, therefore they are almost invisible below 1500 MHz. Therefore, we excluded the 704–1500 MHz portion of the UWL band from all subsequent analyses.

The highest S/N observations were selected to construct a standard template profile for each pulsar. Using these templates, time-of-arrival (TOA) measurements were generated with the PAT utility from the PSRCHIVE package (van Straten et al. 2012) by employing the Fourier-domain Markov Chain Monte Carlo (FDM) algorithm. Also, before creating the TOAs, the archive files were fully scrunched in frequency and polarization and in time they were scrunched such that each corresponding TOAs should have atleast a minimum folded S/N of 15. For PSR J1646–4451, one TOA was extracted per observation, yielding 22 TOAs across 22 epochs. For PSR J1837–0616, multiple TOAs were obtained per observation, resulting in a total of 74 TOAs across 15 epochs.

Time-of-arrival (TOA) measurements were used to derive phase-connected timing solutions using the Pulsar INstrumentation and Timing (PINT; Luo et al. 2021a) software package. All TOAs were corrected to the observatory clock and referenced to the solar system barycenter using the DE440 planetary ephemeris. As the pulsar positions determined from imaging are highly precise, we initially fit only for the spin frequency and its derivative, holding the position fixed at the imaging coordinates. However, we found that fitting for the position as well

² <https://github.com/scottransom/presto>

³ <https://psrrchive.sourceforge.net/>

⁴ <https://pulsar.cgca-hub.org/>

⁵ <https://github.com/v-morello/clfd>

Table 2. Measured and derived timing parameters for PSR J1646–4451 and PSR J1837–0616 with uncertainties within 1σ uncertainties on the last digit. Distances are estimated using both the YMW16 and NE2001 Galactic electron density models.

Parameter	Value	Value
Right Ascension (J2000) ^a	$16^{\text{h}}46^{\text{m}}34\overset{\text{s}}{.}66(1)$	$18^{\text{h}}37^{\text{m}}20\overset{\text{s}}{.}916(6)$
Declination (J2000) ^a	$-44^{\circ}51'23.7(3)''$	$-06^{\circ}16'08.6(6)''$
Start (MJD)	60240.0	60357.9
End (MJD)	60581.1	60684.9
Frequency (Hz)	4.5973495725(6)	8.4610639450(6)
Frequency Derivative (Hz s^{-1})	$-4.574(4) \times 10^{-14}$	$-2.9991(5) \times 10^{-13}$
Epoch of Period (MJD)	60240.0	60391.9
χ^2/DOF	13/17	78/69
RMS residual (μs)	313.7	292.3
Dispersion Measure (pc cm^{-3})	928.0 ± 2	793.7 ± 3
Rotation Measure (rad m^{-2})	–	–
Galactic Longitude (deg)	340.251	25.749
Galactic Latitude (deg)	$+0.305$	$+0.261$
Period (s)	0.21751663305(2)	0.1181884460(1)
Period Derivative (ss^{-1})	$2.1643(1) \times 10^{-15}$	$4.1890(9) \times 10^{-15}$
Characteristic Age (kyr)	1593.4	447.3
Surface Magnetic Field (G)	6.94×10^{11}	7.12×10^{11}
Spin-down Luminosity (erg s^{-1})	8.30×10^{33}	1.00×10^{35}
Distance (kpc)	5.97^a	5.75^a
	9.51^b	8.78^b

^aFrom the YMW16 (Cordes & Lazio 2002) electron density model.

^bFrom the NE2001 (Yao et al. 2017) electron density model.

yielded improved timing solutions. The changes in position after fitting were sub-arcsecond for both pulsars, consistent with the imaging-derived positions. Given the relatively good S/N of all TOAs, no TOAs were excluded from the analysis. We independently verified our timing solutions using TEMPO2 (Edwards et al. 2006), and obtained consistent results, which confirms the robustness of the solutions for both pulsars. The timing residuals are presented in Figure 3, and the corresponding timing parameters are summarized in Table 2. The timing baselines span approximately one year for both pulsars (341 days for PSRJ 1646–4451 and 327 days for PSR J1837–0616), and we therefore further observations are unlikely to significantly improve the precision of the reported solutions.

The pulsars have characteristic ages of 1593 kyr and 447 kyr, respectively, indicating that they are not particularly young and are consistent with the normal pulsar population. The surface magnetic field strengths are approximately 7.0×10^{11} G. The spin-down lumi-

nosities, 8.3×10^{33} erg s $^{-1}$ for PSR J1646–4451 and 1.0×10^{35} erg s $^{-1}$ for PSR J1837–0616, are also typical of the normal pulsar population. The DM-derived distances for both pulsars are \sim 6 kpc using the NE2001 model, and \sim 8.8–9.5 kpc using the YMW16 model. These estimates place both pulsars several kiloparsecs away in the Galactic plane. However, these distance estimates differ by nearly 40%, highlighting the uncertainties in distance determinations from dispersion measures.

3.2. Polarimetry

We performed both flux and polarization calibration for PSR J1646–4451 and PSR J1837–0616 using standard calibration procedure. Each followup pulsar observation was preceded by a short-duration (\sim 2-minute) noise diode observation, which served as a reference for flux and polarization calibration. All observations were first pre-processed for radio-frequency interference (RFI) excision using clfd and then remaining

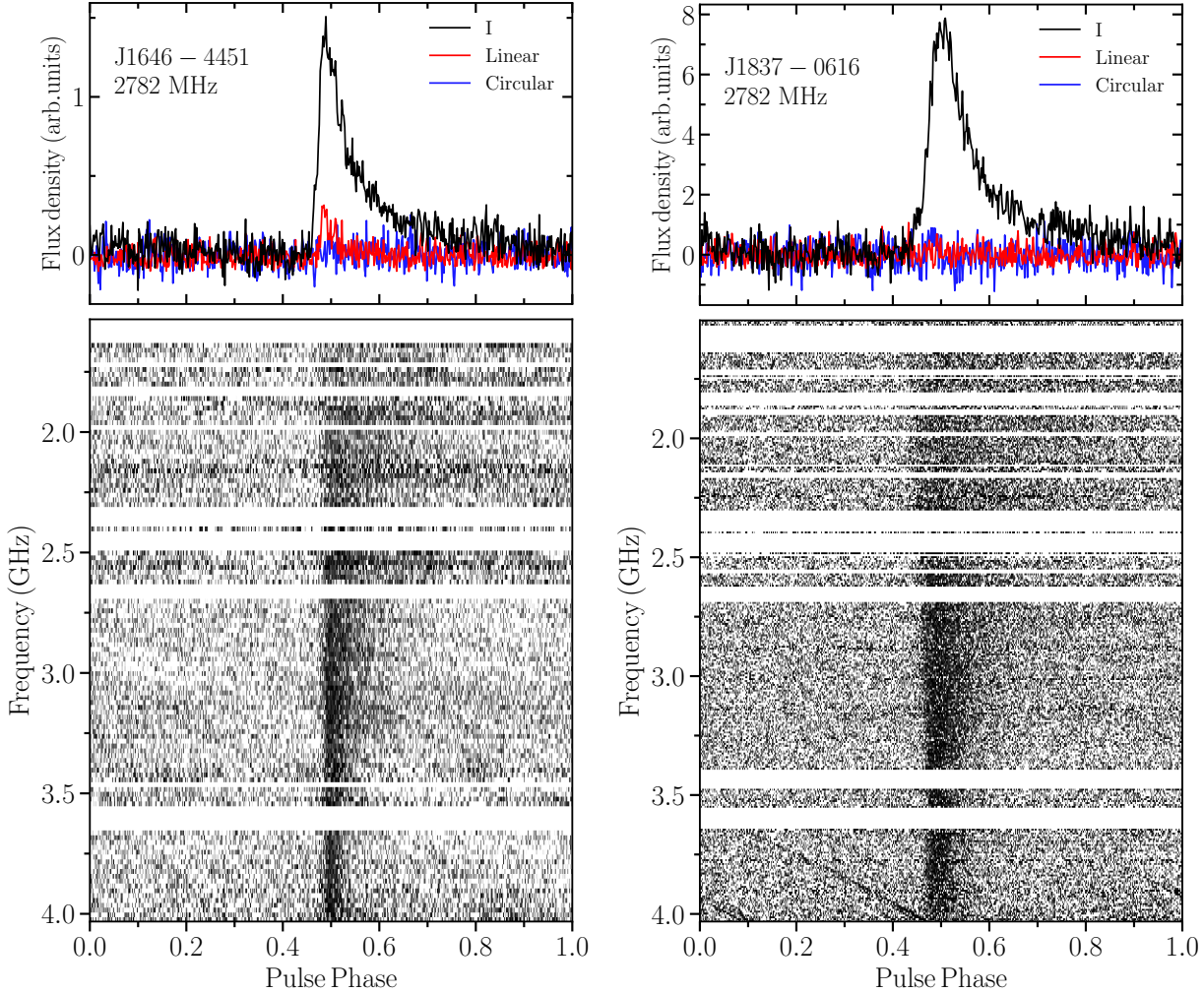


Figure 5. Pulse profiles and frequency-phase diagrams of PSR J1646–4451 (left) and PSR J1837–0616 (right) observed at a central frequency of 2782 MHz. *Top panels*: Total intensity (Stokes I , black), linear polarization (red), and circular polarization (blue) as functions of pulse phase. The profiles are normalized to arbitrary units for comparative visualization. *Bottom panels*: Frequency-resolved dynamic spectra (frequency vs. pulse phase) showing the evolution of pulse structure across the 1.5–4.0 GHz band. Persistent radio-frequency interference (RFI) has been masked in frequency.

bad channels were manually removed using `pazi` routine of PSRCHIVE.

For the flux density reference, we used archival observations of the bright, well-characterized radio quasar PKS B1934–638. This source is regularly monitored as part of the Parkes Pulsar Timing Array project (PPTA; Manchester et al. 2013) and provides a stable reference for the flux density. The `pac` suite of the PSRCHIVE software package was employed to generate the calibrator solution database file from PKS B1934–638 observations. These calibration solutions were then applied to the pulsar observations to obtain fully calibrated Stokes profiles. For each pulsar, individual calibrated observations were coherently co-added to produce a single high signal-to-noise ratio (S/N) profile, preserving both total intensity and polarization information.

We subsequently used the `rmfit` utility within the PSRCHIVE suite to determine the rotation measure (RM) by fitting a Gaussian model to the RM spectrum derived from the frequency-resolved Stokes Q and U parameters. For PSR J1646–4451, we obtained a RM detection of $-134 \pm 7.5 \text{ rad m}^{-2}$ which is typical for pulsars. For PSR J1837–0616, we measured an RM of $1072 \pm 4.26 \text{ rad m}^{-2}$. The Stokes profiles and frequency-versus-phase plots for these pulsars are shown in Figure 5. Based on these pulse profiles, we found that PSR J1646–4451 exhibits approximately 10% linear polarization with no detectable circular polarization, whereas PSR J1837–0616 shows negligible linear or circular polarization. This contrasts with the polarization properties observed in ASKAP imaging, where the circular polarization was found to be 19 % and 7% respec-

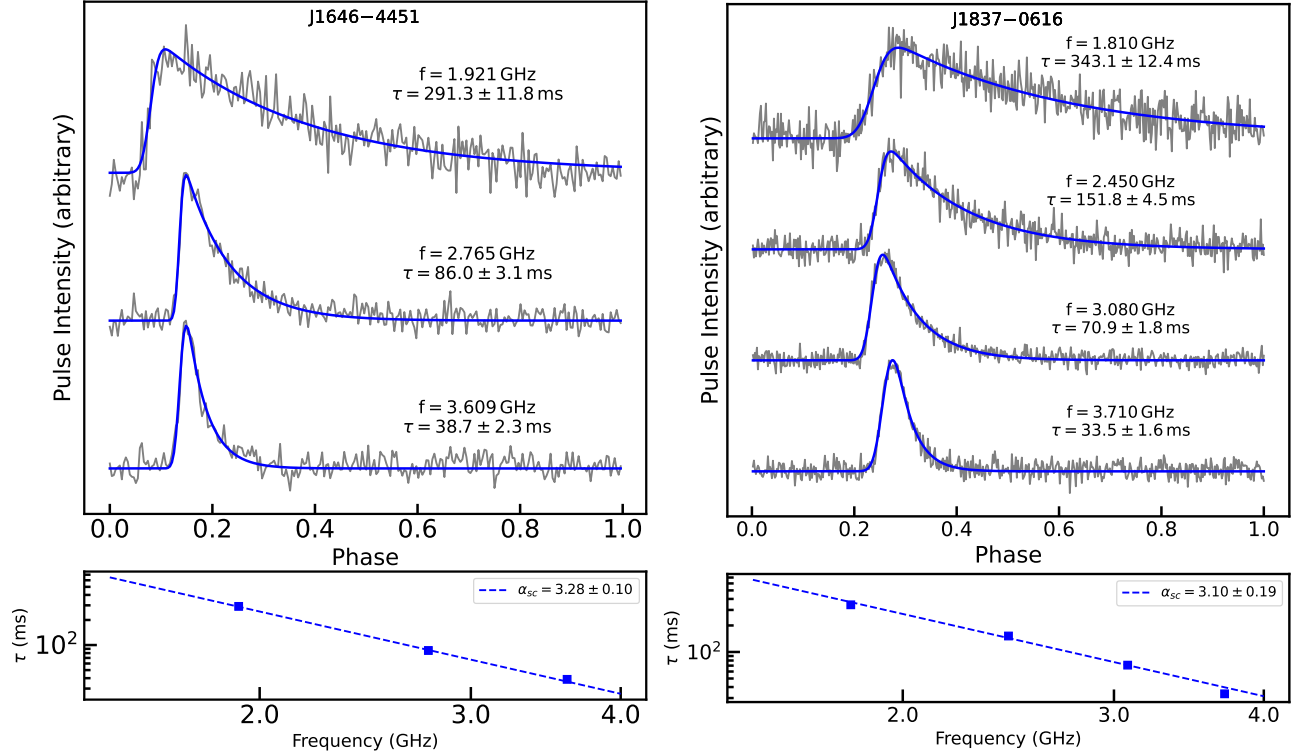


Figure 6. Pulse profiles of PSR J1646–4451 (left) and PSR J1837–0616 (right) at multiple observing frequencies. The grey curves in the upper panels show the observed pulse intensity as a function of rotational phase, while the blue curves represent best-fit models incorporating exponential scattering tails. Each sub-panel indicates the central observing frequency f (in GHz) and the corresponding scattering timescale τ (in ms) with 1σ uncertainties. The profiles exhibit clear frequency-dependent broadening due to interstellar scattering, with larger τ values at lower frequencies. The lower panels display the frequency dependence of the scattering timescales τ in log-log space for each pulsar. The blue dashed lines represent power-law fits of the form $\tau \propto \nu^{-\alpha_{sc}}$, where α_{sc} is the scattering index.

tively. This discrepancy is not surprising and potentially arises from high scattering which can decrease both the linear and circular fractional polarization and even can make them negligible (e.g., Li & Han 2003; Komesaroff et al. 1972).

3.3. Scattering Analysis

Using the co-added observations, we also investigated scattering characteristics of each source across frequency. For this purpose, we divided the coadded observations into several frequency subbands depending on their S/N. For PSR J1646–4451, the total S/N of the coadded profile was 76. We divided the data into three subbands of 844 MHz each, centered at 1920 MHz, 2765 MHz, and 3609 MHz. For PSR J1837–0616, the coadded S/N was 150, and we used four subbands of 633 MHz bandwidth, centered at 1810 MHz, 2450 MHz, 3080 MHz, and 3710 MHz. We fitted an exponential pulse broadening function convolved with a gaussian to each subband profile to extract the scattering timescale

τ_{sc} at each frequency of the form:

$$I(\phi) = I_0 \cdot \exp\left(-\frac{\phi - \phi_0}{\tau_{sc}}\right), \quad \phi > \phi_0,$$

where $I(\phi)$ represents the intensity as a function of pulse phase ϕ , I_0 is the amplitude at reference phase ϕ_0 , and τ_{sc} denotes the scattering timescale characterizing pulse broadening from multipath propagation through the interstellar medium. This model attributes the observed scattering tail to frequency-dependent dispersion effects in the ionized interstellar medium while assuming an intrinsic Gaussian pulse shape. The resulting frequency-dependent scattering timescales for both pulsars are presented in Figure 5.

For PSR J1646–4451, the measured scattering timescales were 291.3 ± 11.8 ms at 1.921 GHz, 86.0 ± 3.1 ms at 2.765 GHz, and 38.7 ± 2.3 ms at 3.609 GHz. For PSR J1837–0616, we obtained 342.4 ± 12.4 ms at 1.810 GHz, 151.9 ± 4.5 ms at 2.450 GHz, 70.9 ± 1.8 ms at 3.080 GHz, and 33.5 ± 1.6 ms at 3.710 GHz. We modeled the frequency dependence of the scattering timescale using a power-law:

$$\tau_{\text{sc}}(f) = \tau_0 \left(\frac{f}{1 \text{ GHz}} \right)^{-\alpha},$$

where τ_0 is the scattering timescale at 1 GHz and α is the scattering index. A weighted least-squares fit yielded a scattering index of $\alpha = 3.28 \pm 0.10$ for PSR J1646–4451 and $\alpha = 3.10 \pm 0.19$ for PSR J1837–0616. These values are somewhat flatter than the Kolmogorov turbulence prediction of ($\alpha \sim 4.0$; Lee & Jokipii 1976), potentially indicating deviations from homogeneous isotropic scattering media or the presence of anisotropic or truncated scattering screens.

Using the measured scattering indices, the extrapolated scattering timescales at 1 GHz are $\tau_{\text{sc}}(1 \text{ GHz}) = 2479 \text{ ms}$ for PSR J1646–4451 and $\tau_{\text{sc}}(1 \text{ GHz}) = 2154 \text{ ms}$ for PSR J1837–0616. These values indicate that both pulsars are among the highest scattered pulsar population, and consistent with expectations for sources located along dense or turbulent lines of sight in the Galactic plane. These scattering timescale values are plotted in Figure 7, along with the empirical relation from Bhat et al. (2004) and Cordes et al. (2022). The scattering timescale for PSR J1646–4451 is in good agreement with the Bhat et al. (2004) model, differing by only 6%. In contrast, the timescale for PSR J1837–0616 at 1 GHz is significantly higher—approximately 2.25 times larger—than the predicted value which is expected given the substantial intrinsic scatter and uncertainties inherent in such empirical models.

4. DISCUSSION

No new pulsations were detected in the periodicity searches of the remaining two circularly polarized sources. One of those is likely associated with a star. The nature of the other source, J1832–0808, is less clear. However, one known pulsar, PSR B1829–08, was detected in the observation of that source. PSR B1829–08 is a bright pulsar with a well-determined position and timing solution. It lies approximately 19' from the beam center. Given both its brightness and the size of the Parkes beam ($\approx 28'$), it is likely that this detection is due to a side-lobe response, rather than a physical association with the circularly polarized source. Bright pulsars like B1829–08 can also often be detected at relatively large off-axis angles.

The apparent lack of pulsations in J1832–0808, despite its continuum properties being similar to those of pulsars, motivated us to investigate whether the pulsations could be missed somehow. Although it's $|V|/I$ is about 3 time the average $|V|/I$ observed in pulsars, it is consistent with circular polarization values detected in

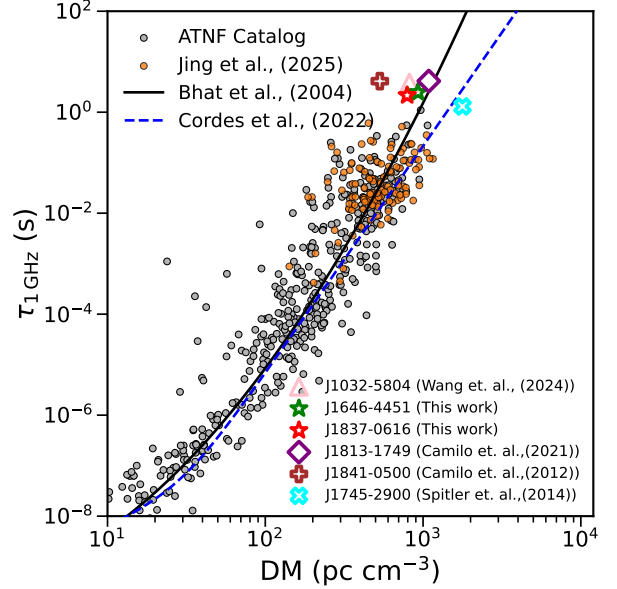


Figure 7. Measured scattering timescales at 1 GHz $\tau_{1 \text{ GHz}}$ as a function of dispersion measure (DM) for a sample of pulsars. Grey circles represent archival measurements from the PSRCAT, and orange circles corresponds to the published $\tau_{1 \text{ GHz}}$ of pulsars discovered in FAST GPPS survey (Jing et al. 2025). The solid black line and dashed blue line denote the empirical relations from Bhat et al. (2004) and (Cordes et al. 2022), showing the expected dependence of scattering on DM. The green and red star mark the locations of PSR J1646–4451 and PSR J1837–0616, respectively, as determined from our scattering analysis. Both sources lie near the upper envelope of the distribution, indicating relatively strong scattering along their lines of sight.

the known pulsar population in the Rapid ASKAP Continuum Survey (Anumarpudi et al. 2023). Its mean Stokes I flux density is approximately 2.4 mJy at 843–943.5 MHz. Scaling the flux density to 1.4 GHz, and assuming a steep spectral index of -2.0 , its expected flux density at 1.4 GHz would be $\sim 1.0 \text{ mJy}$. Furthermore, based on the available ASKAP epochs, its total intensity and circular polarization appear stable over time, with no strong evidence of variability (see Figure 2). These properties are broadly consistent with typical radio pulsars. However, the mean signal-to-noise ratio (S/N) for this source is relatively low as compared to the confirmed pulsars in the sample,. One plausible explanation for the non-detection of these sources in follow-up searches is that it is simply too faint to be detected in the ~ 1 hour Parkes observations.

To evaluate this, we considered the flux-density sensitivity curves for the Parkes telescope at L-band (center frequency: 1250 MHz, bandwidth: 500 MHz) for a 1.2-hour integration. In the absence of scattering, pulsars with spin periods $> 100 \text{ ms}$, flux densities $\gtrsim 0.1 \text{ mJy}$,

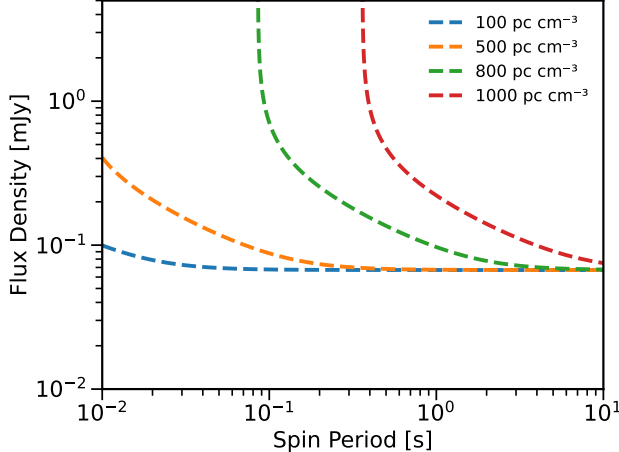


Figure 8. Minimum detectable flux density as a function of pulsar spin period for various dispersion measures (DMs), assuming a fixed Parkes observing setup with a central frequency of 1400 MHz, bandwidth of 500 MHz, and an integration time of 1 hour. Sensitivity curves are shown for DMs of 100, 500, 800, and 1000 pc cm⁻³. The effective pulse width used in computing these curves is given by $W_{\text{eff}} = \sqrt{W_{\text{int}}^2 + \tau_{\text{scat}}^2}$, where W_{int} is the intrinsic pulse width, corresponds to a 5% duty cycle, and τ_{scat} is the scattering timescale estimated for the DMs using the empirical relation from Bhat et al. (2004). At higher DMs, sensitivity to fast pulsars is significantly degraded due to dispersion and scattering effects, illustrating the observational bias against detecting short-period pulsars in high-DM environments.

and DMs $\lesssim 1500 \text{ cm}^{-3} \text{ pc}$ should be detectable. However, when accounting for scattering using the empirical relation from Bhat et al. (2004), pulsars with periods $< 200 \text{ ms}$, DMs $> 800 \text{ cm}^{-3} \text{ pc}$, and flux densities $\lesssim 0.2 \text{ mJy}$ may fall below the detection threshold due to significant pulse broadening at L-band (see Figure 8). Therefore, if J1832–0808 is indeed a pulsar, its non-detection could be attributed to several factors: it may be fast-spinning ($P < 100 \text{ ms}$), lie at high DM ($> 800 \text{ cm}^{-3} \text{ pc}$), and suffer from severe scattering, rendering it undetectable at L-band. Unlike the two confirmed pulsars, this source may be intrinsically faint and possess steeper radio spectra. Given these considerations, future searches with high-sensitivity, lower-frequency telescopes such as MeerKAT would be particularly valuable for confirming the nature of these sources.

Given the optical/NIR+radio analysis presented above, three of which resulted in non-detections (or accidental associations), we adopted a phenomenological approach to understand the nature of J1832–0808 and by comparing their radio and K_s -band properties. Figure 9 shows different source classes that emit significantly polarized radio emission, on the phase space of their polar-

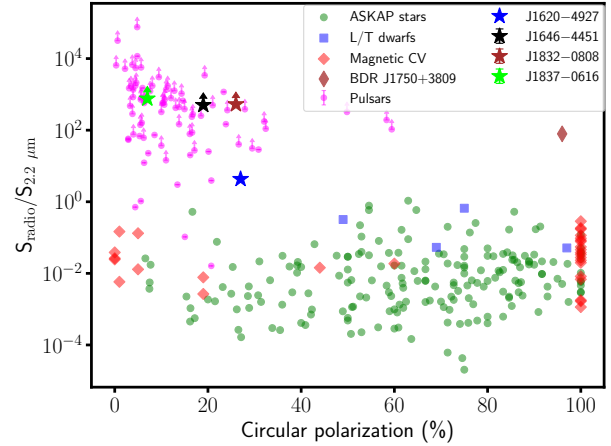


Figure 9. Phase space of circular polarization fraction and the relative source strength in radio and K_s bands showing different populations of sources (also see Wang et al. 2022). The green circles represent radio-detected stars (Driessen et al. 2024a), the red diamonds represent MCVs (Barrett et al. 2020), the blue squares show dwarf stars (Pritchard et al. 2021), and the pink circles represent pulsars. Individual sources of interest, including the radio-discovered brown dwarf BDR J0750+3809 (Vedantham et al. 2020) and our sample, are highlighted.

ization properties and the relative radio to K_s -band continuum strength. It can be seen that J1620–4927, a radio star, has a similar radio-to-NIR flux ratio a factor of > 10 more extreme than most stars selected from a circular polarization search (Pritchard et al. 2021), but it is consistent with the radio-discovered brown dwarf BDR J0750+3809 (Vedantham et al. 2020) even though they have very different spectral types and polarization levels. This may suggest that stars when identified through radio discovery may span a wider range of properties than previously thought. The other three sources in our sample lie in a region occupied by pulsars, suggesting that J1832–0808 may indeed be a pulsar despite the lack of detected pulsations.

5. CONCLUSIONS

We report the discovery of two highly scattered pulsars, PSRs J1646–4451 and J1837–0616, identified through their circular polarization in ASKAP continuum images and confirmed via targeted observations with the Parkes Ultra-Wideband Low (UWL) receiver. Both PSR J1646–4451 and PSR J1837–0616 exhibit spin characteristics that are typical of the normal pulsar population. Their spin periods—217 ms for PSR J1646–4451 and 118 ms for PSR J1837–0616 place them within the region of the P – \dot{P} diagram that is commonly occupied by young pulsars, including those associated with supernova remnants. However, their period

derivatives are consistent with the broader population of normal, non-recycled pulsars. PSR J1646–4451 has a characteristic age of approximately 1.59 Myr, while PSR J1837–0616 is relatively younger, with a characteristic age of about 0.44 Myr. Despite the latter’s lower age, it does not fall into the category of truly young pulsars, which are typically much younger (< 50 kyr) and often show direct associations with supernova remnants.

In addition to their typical spin properties, both pulsars exhibit high dispersion measures (DMs) and exceptional scattering characteristics. Their frequency-dependent scattering timescales (Figure 6) yield scattering indices of $\alpha_{\text{sc}} = 3.28$ and $\alpha_{\text{sc}} = 3.1$, which are flatter than the canonical $\alpha_{\text{sc}} = 4$ expected for Kolmogorov turbulence. Their scattering timescales at 1 GHz—2479 ms for PSR J1646–4451 and 2154 ms for PSR J1837–0616—place them among the five most heavily scattered pulsars known. Among the top five scattered pulsars, PSR J1813–1749 was first detected in X-rays within the supernova remnant G12.82–0.02 and later confirmed through high-frequency radio observations, exhibiting a scattering timescale of 4.14 s at 1 GHz (Camilo et al. 2021). The second, PSR J1841–0500 (Camilo et al. 2012), shows a comparable scattering timescale of 4.12 s at 1 GHz. Notably, the remaining three pulsars—including the two reported here and PSR J1032–5804—were all initially identified as compact, circularly polarized sources in ASKAP imaging.

This emerging trend strongly suggests that identifying pulsar candidates using image-domain polarization search techniques and confirming them using wideband receivers serves as a powerful diagnostic for uncovering unusual pulsars particularly pulsars in high-DM, inner-Galactic regions where scattering is most severe.

Many of the sources identified through this method may represent a population of pulsars that are intrinsically young, rapidly spinning, or members of binary systems—categories that are often underrepresented in traditional pulsar surveys due to extreme scattering and associated selection biases. The discovery of two pulsars from four candidates (a 50% success rate) further validates circular polarization as an efficient discriminant for pulsar searches in imaging surveys. Traditional periodicity searches at $\nu < 2$ GHz would likely have missed these sources due to scattering smearing exceeding their spin periods. This approach complements time-domain surveys by probing populations in regions of high interstellar medium (ISM) turbulence, where $\tau_{\text{sc}} \propto \nu^{-\alpha}$ suppresses low-frequency detections. Similar strategies have uncovered other highly scattered pulsars (e.g., PSR J1638–4713; Lazarević et al. 2024), underscoring the ne-

cessity of wideband receivers like UWL to detect high-frequency signals above the scattering horizon.

The severe scattering observed towards these pulsars may be attributed to their locations relative to nearby HII regions. Both J1646–4451 and J1837–0616 lie on the edge of large Galactic HII regions, as seen by the Widefield Infrared Survey Explorer (WISE; Wright et al. 2010). The two regions are seen in Fig. 1 as $\sim 20'$ -diameter, shell-like structures; respectively these pulsars are closest to WISE G340.216+00.424 and WISE G025.867+00.118. The pulsars are apparently coincident with the edge of the 12 μm emission derived from the UV fluorescence of polycyclic aromatic hydrocarbons typically found around HII regions. No reliable distance estimates are available in the literature for these sources, although we may make an estimate based on their size. The median HII region diameter in the WISE HII catalogue (Anderson et al. 2014) is ~ 3 pc, which would place these objects ~ 500 pc away. This is consistent with the low-frequency (free-free) absorption signal seen in the GaLactic and Extragalactic All-sky Murchison Widefield Array (GLEAM; Wayth et al. 2015; Hurley-Walker et al. 2019) and GLEAM-eXtended (GLEAM-X; Hurley-Walker et al. 2022, Mantovanini et al. accepted) data toward these objects.

HII regions have been seen to increase the level of scattering for pulsars detected behind them, along the line-of-sight (e.g. Dennison et al. 1984). A similar effect could be at play here, and would be maximised if these pulsars lie at twice the distance of the intervening HII regions. Careful modelling and high-quality data on both the pulsars and the HII region can be used to solve for the intrinsic properties of the sources (see e.g. Sicheneder & Dexter 2017) but this lies beyond the scope of this paper.

Current and future large-scale radio imaging projects, such as an ongoing EMU survey with ASKAP and surveys with upcoming SKA, and DSA-2000 telescopes, are poised to substantially broaden the parameter space for pulsar discoveries by leveraging radio imaging. These capabilities will be especially valuable for detecting pulsars obscured by scattering in the Galactic plane, which remain challenging to traditional time-domain searches. Crucially, wide-band follow-up observations will play an instrumental role in confirming such candidates and characterizing their properties, particularly for systems all types of pulsars embedded in dense environments. Collectively, these developments highlight the complementary strengths of imaging and time-domain methodologies in uncovering diverse neutron star populations. Polarized continuum surveys, in particular, are emerging as a powerful tool for completing the Galactic pulsar

inventory and probing small-scale structure in the turbulent interstellar medium. At the same time, these advances underscore the continued need for improved scattering models of radio wave propagation through highly scattered regions.

Upcoming SKA-era continuum surveys such as EMU and DSA-2000 are poised to substantially broaden the parameter space for pulsar discovery by leveraging radio imaging. These capabilities will be especially valuable for detecting pulsars obscured by scattering in the Galactic plane, which remain challenging to traditional time-domain searches. Crucially, wide-band follow-up observations will play an instrumental role in confirming such candidates and characterizing their properties, particularly for systems all types of pulsars embedded in dense environments. Collectively, these developments highlight the complementary strengths of imaging and time-domain methodologies in uncovering diverse neutron star populations. Polarized continuum surveys, in particular, are emerging as a powerful tool for completing the Galactic pulsar inventory and probing small-scale structure in the turbulent interstellar medium. At the same time, these advances underscore the continued need for improved scattering models of radio wave propagation through highly scattered regions.

R.S. acknowledges the continuing valuable support of the Max Planck Society and support from NSF grant AST-1816904. D.K. is supported by NSF grants AST-1816492, AST-1816904, and AST-2511757. N.H.-W. is the recipient of an Australian Research Council Future Fellowship (project number FT190100231). This scientific work uses data obtained from Inyarrimanha Ilgari Bundara/the Murchison Radio-astronomy Observatory. We acknowledge the Wajarri Yamaji People as the Traditional Owners and native title holders of the Observatory site. CSIRO's ASKAP radio telescope is part of the Australia Telescope National Facility (<https://ror.org/05qajvd42>). Operation of ASKAP is funded by the Australian Government with support from the National Collaborative Research Infrastructure Strategy. ASKAP uses the resources of the Pawsey Supercomputing Research Centre. Establishment of ASKAP, Inyarrimanha Ilgari Bundara, the CSIRO Murchison Radio-astronomy Observatory, and the Pawsey Supercomputing Research Centre are initiatives of the Australian Government, with support from the Government of Western Australia and the Science and Industry Endowment Fund. The Parkes radio telescope is part of the Australia Telescope National Facility, funded by the Australian Government for operation as a National Facility managed by CSIRO. We acknowledge the Wiradjuri People as the Traditional Owners of the Parkes Observatory site. The Australia Telescope Compact Array is also part of the Australia Telescope National Facility (<https://ror.org/05qajvd42>), and we acknowledge the Gomeroloi People as the Traditional Owners of its site. Parts of this research were supported by the Australian Research Council Centre of Excellence for

Facilities: ASKAP, Parkes, WISE (<https://www.ipac.caltech.edu/doi/irsa/10.26131/IRSA153>), ATCA, VST.

Software: astropy (Astropy Collaboration et al. 2013, 2018), PINT (Luo et al. 2021b), PSRCHIVE (Hotan et al. 2004), Pulsar Survey Scraper (Kaplan 2022), PyGEDM (Price et al. 2021).

REFERENCES

Ahmad, A., Dai, S., Lazarević, S., et al. 2025, MNRAS, 537, 2868, doi: [10.1093/mnras/staf181](https://doi.org/10.1093/mnras/staf181)

Anderson, L. D., Bania, T. M., Balser, D. S., et al. 2014, ApJS, 212, 1, doi: [10.1088/0067-0049/212/1/1](https://doi.org/10.1088/0067-0049/212/1/1)

Anumarlapudi, A., Ehlke, A., Jones, M. L., et al. 2023, ApJ, 956, 28, doi: [10.3847/1538-4357/aceb5d](https://doi.org/10.3847/1538-4357/aceb5d)

Astropy Collaboration, Robitaille, T. P., Tollerud, E. J., et al. 2013, A&A, 558, A33, doi: [10.1051/0004-6361/201322068](https://doi.org/10.1051/0004-6361/201322068)

Astropy Collaboration, Price-Whelan, A. M., Sipőcz, B. M., et al. 2018, AJ, 156, 123, doi: [10.3847/1538-3881/aabc4f](https://doi.org/10.3847/1538-3881/aabc4f)

Barrett, P., Dieck, C., Beasley, A. J., Mason, P. A., & Singh, K. P. 2020, Advances in Space Research, 66, 1226, doi: [10.1016/j.asr.2020.04.007](https://doi.org/10.1016/j.asr.2020.04.007)

Best, P. N., Kondapally, R., Williams, W. L., et al. 2023, MNRAS, 523, 1729, doi: [10.1093/mnras/stad1308](https://doi.org/10.1093/mnras/stad1308)

Bhat, N. D. R., Cordes, J. M., Camilo, F., Nice, D. J., & Lorimer, D. R. 2004, ApJ, 605, 759, doi: [10.1086/382680](https://doi.org/10.1086/382680)

Bjornsson, C. I. 1990, MNRAS, 242, 158, doi: [10.1093/mnras/242.2.158](https://doi.org/10.1093/mnras/242.2.158)

Camilo, F., Ransom, S. M., Chatterjee, S., Johnston, S., & Demorest, P. 2012, ApJ, 746, 63, doi: [10.1088/0004-637X/746/1/63](https://doi.org/10.1088/0004-637X/746/1/63)

Camilo, F., Ransom, S. M., Halpern, J. P., & Roshi, D. A. 2021, ApJ, 917, 67, doi: [10.3847/1538-4357/ac0720](https://doi.org/10.3847/1538-4357/ac0720)

Catelan, M., Minniti, D., Lucas, P. W., et al. 2011, in RR Lyrae Stars, Metal-Poor Stars, and the Galaxy, ed. A. McWilliam, Vol. 5, 145, doi: [10.48550/arXiv.1105.1119](https://doi.org/10.48550/arXiv.1105.1119)

Chambers, K. C., Magnier, E. A., Metcalfe, N., et al. 2016, arXiv e-prints, arXiv:1612.05560, doi: [10.48550/arXiv.1612.05560](https://doi.org/10.48550/arXiv.1612.05560)

Cordes, J. M., & Lazio, T. J. W. 2002, arXiv e-prints, astro, doi: [10.48550/arXiv.astro-ph/0207156](https://doi.org/10.48550/arXiv.astro-ph/0207156)

Cordes, J. M., Ocker, S. K., & Chatterjee, S. 2022, ApJ, 931, 88, doi: [10.3847/1538-4357/ac6873](https://doi.org/10.3847/1538-4357/ac6873)

Cordes, J. M., Freire, P. C. C., Lorimer, D. R., et al. 2006, ApJ, 637, 446, doi: [10.1086/498335](https://doi.org/10.1086/498335)

Dai, S., Johnston, S., & Hobbs, G. 2018, in IAU Symposium, Vol. 337, Pulsar Astrophysics the Next Fifty Years, ed. P. Weltevrede, B. B. P. Perera, L. L. Preston, & S. Sanidas, 328–329, doi: [10.1017/S1743921317008833](https://doi.org/10.1017/S1743921317008833)

Dennison, B., Thomas, M., Booth, R. S., et al. 1984, A&A, 135, 199

Driessen, L. N., Pritchard, J., Murphy, T., et al. 2024a, PASA, 41, e084, doi: [10.1017/pasa.2024.72](https://doi.org/10.1017/pasa.2024.72)

—. 2024b, PASA, 41, e084, doi: [10.1017/pasa.2024.72](https://doi.org/10.1017/pasa.2024.72)

Edwards, R. T., Hobbs, G. B., & Manchester, R. N. 2006, MNRAS, 372, 1549, doi: [10.1111/j.1365-2966.2006.10870.x](https://doi.org/10.1111/j.1365-2966.2006.10870.x)

Fender, R., Woudt, P. A., Corbel, S., et al. 2016, in MeerKAT Science: On the Pathway to the SKA, 13, doi: [10.22323/1.277.0013](https://doi.org/10.22323/1.277.0013)

Frail, D. A., Polisensky, E., Hyman, S. D., et al. 2024, ApJ, 975, 34, doi: [10.3847/1538-4357/ad74fd](https://doi.org/10.3847/1538-4357/ad74fd)

Gaia Collaboration, Vallenari, A., Brown, A. G. A., et al. 2023, A&A, 674, A1, doi: [10.1051/0004-6361/202243940](https://doi.org/10.1051/0004-6361/202243940)

Han, J. L., Wang, C., Wang, P. F., et al. 2021, Research in Astronomy and Astrophysics, 21, 107, doi: [10.1088/1674-4527/21/5/107](https://doi.org/10.1088/1674-4527/21/5/107)

Hobbs, G., Manchester, R. N., Dunning, A., et al. 2020, PASA, 37, e012, doi: [10.1017/pasa.2020.2](https://doi.org/10.1017/pasa.2020.2)

Hotan, A. W., van Straten, W., & Manchester, R. N. 2004, PASA, 21, 302, doi: [10.1071/AS04022](https://doi.org/10.1071/AS04022)

Hurley-Walker, N., Hancock, P. J., Franzen, T. M. O., et al. 2019, PASA, 36, e047, doi: [10.1017/pasa.2019.37](https://doi.org/10.1017/pasa.2019.37)

Hurley-Walker, N., Galvin, T. J., Duchesne, S. W., et al. 2022, PASA, 39, e035, doi: [10.1017/pasa.2022.17](https://doi.org/10.1017/pasa.2022.17)

Jankowski, F., van Straten, W., Keane, E. F., et al. 2018, MNRAS, 473, 4436, doi: [10.1093/mnras/stx2476](https://doi.org/10.1093/mnras/stx2476)

Jing, W. C., Han, J. L., Wang, C., et al. 2025, arXiv e-prints, arXiv:2506.14519, doi: [10.48550/arXiv.2506.14519](https://doi.org/10.48550/arXiv.2506.14519)

Johnston, H. M., & Kulkarni, S. R. 1991, ApJ, 368, 504, doi: [10.1086/169715](https://doi.org/10.1086/169715)

Kaplan, D. L. 2022, PSS: Pulsar Survey Scraper, Astrophysics Source Code Library, record ascl:2210.001. <http://ascl.net/2210.001>

Kaplan, D. L., Dai, S., Lenc, E., et al. 2019, ApJ, 884, 96, doi: [10.3847/1538-4357/ab397f](https://doi.org/10.3847/1538-4357/ab397f)

Keane, E. F., & McLaughlin, M. A. 2011, Bulletin of the Astronomical Society of India, 39, 333, doi: [10.48550/arXiv.1109.6896](https://doi.org/10.48550/arXiv.1109.6896)

Keane, E. F., Barr, E. D., Jameson, A., et al. 2018, MNRAS, 473, 116, doi: [10.1093/mnras/stx2126](https://doi.org/10.1093/mnras/stx2126)

Keith, M. J., Jameson, A., van Straten, W., et al. 2010, MNRAS, 409, 619, doi: [10.1111/j.1365-2966.2010.17325.x](https://doi.org/10.1111/j.1365-2966.2010.17325.x)

Komesaroff, M. M., Hamilton, P. A., & Ables, J. G. 1972, Australian Journal of Physics, 25, 759, doi: [10.1071/PH720759](https://doi.org/10.1071/PH720759)

Lacy, M., Baum, S. A., Chandler, C. J., et al. 2020, PASP, 132, 035001, doi: [10.1088/1538-3873/ab63eb](https://doi.org/10.1088/1538-3873/ab63eb)

Lawrence, A., Warren, S. J., Almaini, O., et al. 2007, MNRAS, 379, 1599, doi: [10.1111/j.1365-2966.2007.12040.x](https://doi.org/10.1111/j.1365-2966.2007.12040.x)

Lazarević, S., Filipović, M. D., Dai, S., et al. 2024, PASA, 41, e032, doi: [10.1017/pasa.2024.13](https://doi.org/10.1017/pasa.2024.13)

Lee, L. C., & Jokipii, J. R. 1976, ApJ, 206, 735, doi: [10.1086/154434](https://doi.org/10.1086/154434)

Lenc, E., Murphy, T., Lynch, C. R., Kaplan, D. L., & Zhang, S. N. 2018, MNRAS, 478, 2835, doi: [10.1093/mnras/sty1304](https://doi.org/10.1093/mnras/sty1304)

Li, X. H., & Han, J. L. 2003, A&A, 410, 253, doi: [10.1051/0004-6361:20031190](https://doi.org/10.1051/0004-6361:20031190)

Lorimer, D. R., & Kramer, M. 2004, Handbook of Pulsar Astronomy, Vol. 4

Luo, J., Ransom, S., Demorest, P., et al. 2021a, ApJ, 911, 45, doi: [10.3847/1538-4357/abe62f](https://doi.org/10.3847/1538-4357/abe62f)

—. 2021b, ApJ, 911, 45, doi: [10.3847/1538-4357/abe62f](https://doi.org/10.3847/1538-4357/abe62f)

Manchester, R. N., Lyne, A. G., Camilo, F., et al. 2001, MNRAS, 328, 17, doi: [10.1046/j.1365-8711.2001.04751.x](https://doi.org/10.1046/j.1365-8711.2001.04751.x)

Manchester, R. N., Hobbs, G., Bailes, M., et al. 2013, PASA, 30, e017, doi: [10.1017/pasa.2012.017](https://doi.org/10.1017/pasa.2012.017)

McConnell, D., Hale, C. L., Lenc, E., et al. 2020, PASA, 37, e048, doi: [10.1017/pasa.2020.41](https://doi.org/10.1017/pasa.2020.41)

McLaughlin, M. A., Lyne, A. G., Lorimer, D. R., et al. 2006, Nature, 439, 817, doi: [10.1038/nature04440](https://doi.org/10.1038/nature04440)

Mcsweeney, S. J., Moseley, J., Hurley-Walker, N., et al. 2025, ApJ, 981, 143, doi: [10.3847/1538-4357/adb27f](https://doi.org/10.3847/1538-4357/adb27f)

Murphy, T., Chatterjee, S., Kaplan, D. L., et al. 2013, PASA, 30, e006, doi: [10.1017/pasa.2012.006](https://doi.org/10.1017/pasa.2012.006)

Murphy, T., Kaplan, D. L., Stewart, A. J., et al. 2021, PASA, 38, e054, doi: [10.1017/pasa.2021.44](https://doi.org/10.1017/pasa.2021.44)

Norris, R. P., Hopkins, A. M., Afonso, J., et al. 2011, PASA, 28, 215, doi: [10.1071/AS11021](https://doi.org/10.1071/AS11021)

Oswald, L. S., Johnston, S., Karastergiou, A., et al. 2023, MNRAS, 520, 4961, doi: [10.1093/mnras/stad070](https://doi.org/10.1093/mnras/stad070)

Padmanabhan, P. V., Barr, E. D., Sridhar, S. S., et al. 2023, MNRAS, 524, 1291, doi: [10.1093/mnras/stad1900](https://doi.org/10.1093/mnras/stad1900)

Price, D. C., Flynn, C., & Deller, A. 2021, PASA, 38, e038, doi: [10.1017/pasa.2021.33](https://doi.org/10.1017/pasa.2021.33)

Pritchard, J., Murphy, T., Zic, A., et al. 2021, MNRAS, 502, 5438, doi: [10.1093/mnras/stab299](https://doi.org/10.1093/mnras/stab299)

Rickett, B. J. 1977, ARA&A, 15, 479, doi: [10.1146/annurev.aa.15.090177.002403](https://doi.org/10.1146/annurev.aa.15.090177.002403)

—. 1990, ARA&A, 28, 561, doi: [10.1146/annurev.aa.28.090190.003021](https://doi.org/10.1146/annurev.aa.28.090190.003021)

Saikia, D. J., & Salter, C. J. 1988, ARA&A, 26, 93, doi: [10.1146/annurev.aa.26.090188.000521](https://doi.org/10.1146/annurev.aa.26.090188.000521)

Sanidas, S., Cooper, S., Bassa, C. G., et al. 2019, A&A, 626, A104, doi: [10.1051/0004-6361/201935609](https://doi.org/10.1051/0004-6361/201935609)

Saydjari, A. K., Schlafly, E. F., Lang, D., et al. 2023, ApJS, 264, 28, doi: [10.3847/1538-4365/aca594](https://doi.org/10.3847/1538-4365/aca594)

Sengar, R., Bailes, M., Balakrishnan, V., et al. 2023, MNRAS, 522, 1071, doi: [10.1093/mnras/stad508](https://doi.org/10.1093/mnras/stad508)

—. 2025, MNRAS, 536, 3159, doi: [10.1093/mnras/stae2716](https://doi.org/10.1093/mnras/stae2716)

Sicheneder, E., & Dexter, J. 2017, MNRAS, 467, 3642, doi: [10.1093/mnras/stx103](https://doi.org/10.1093/mnras/stx103)

Sobey, C., Bassa, C. G., O'Sullivan, S. P., et al. 2022, A&A, 661, A87, doi: [10.1051/0004-6361/202142636](https://doi.org/10.1051/0004-6361/202142636)

Staelin, D. H. 1969, IEEE Proceedings, 57, 724, doi: [10.1109/PROC.1969.7051](https://doi.org/10.1109/PROC.1969.7051)

Stovall, K., Lynch, R. S., Ransom, S. M., et al. 2014, ApJ, 791, 67, doi: [10.1088/0004-637X/791/1/67](https://doi.org/10.1088/0004-637X/791/1/67)

Sutton, J. M. 1971, MNRAS, 155, 51, doi: [10.1093/mnras/155.1.51](https://doi.org/10.1093/mnras/155.1.51)

Thompson, C., Blandford, R. D., Evans, C. R., & Phinney, E. S. 1994, ApJ, 422, 304, doi: [10.1086/173728](https://doi.org/10.1086/173728)

van Straten, W., Demorest, P., & Oslowski, S. 2012, Astronomical Research and Technology, 9, 237, doi: [10.48550/arXiv.1205.6276](https://doi.org/10.48550/arXiv.1205.6276)

Vedantham, H. K., Callingham, J. R., Shimwell, T. W., et al. 2020, ApJL, 903, L33, doi: [10.3847/2041-8213/abc256](https://doi.org/10.3847/2041-8213/abc256)

Wang, N., Manchester, R. N., & Johnston, S. 2007, MNRAS, 377, 1383, doi: [10.1111/j.1365-2966.2007.11703.x](https://doi.org/10.1111/j.1365-2966.2007.11703.x)

Wang, P. F., Han, J. L., Xu, J., et al. 2023, Research in Astronomy and Astrophysics, 23, 104002, doi: [10.1088/1674-4527/ace1f](https://doi.org/10.1088/1674-4527/ace1f)

Wang, Y., Murphy, T., Kaplan, D. L., et al. 2022, ApJ, 930, 38, doi: [10.3847/1538-4357/ac61dc](https://doi.org/10.3847/1538-4357/ac61dc)

Wang, Z., Kaplan, D. L., Sengar, R., et al. 2024, ApJ, 961, 175, doi: [10.3847/1538-4357/ad0fe8](https://doi.org/10.3847/1538-4357/ad0fe8)

Wayth, R. B., Lenc, E., Bell, M. E., et al. 2015, PASA, 32, e025, doi: [10.1017/pasa.2015.26](https://doi.org/10.1017/pasa.2015.26)

Wright, E. L., Eisenhardt, P. R. M., Mainzer, A. K., et al. 2010, AJ, 140, 1868, doi: [10.1088/0004-6256/140/6/1868](https://doi.org/10.1088/0004-6256/140/6/1868)

Yao, J. M., Manchester, R. N., & Wang, N. 2017, ApJ, 835, 29, doi: [10.3847/1538-4357/835/1/29](https://doi.org/10.3847/1538-4357/835/1/29)

Zhu, X., Zhang, Z., Zhao, C., et al. 2024, MNRAS, 529, 1082, doi: [10.1093/mnras/stae331](https://doi.org/10.1093/mnras/stae331)

Zic, A., Wang, Z., Lenc, E., et al. 2024, MNRAS, 528, 5730, doi: [10.1093/mnras/stae033](https://doi.org/10.1093/mnras/stae033)